Quantum heat bath for spin-lattice dynamics

C. H. Woo,[1,*] Haohua Wen,[1] A. A. Semenov,[1,2] S. L. Dudarev,[3] and Pui-Wai Ma[3]

[1]*Department of Physics and Materials Science, City University of Hong Kong, Kowloon, Hong Kong SAR, China*

[2]*Institute for Nuclear Research, Russian Academy of Sciences, Moscow, Russia*

[3]*CCFE, Culham Science Centre, Oxfordshire OX14 3DB, United Kingdom*

(Received 16 November 2014; revised manuscript received 17 February 2015; published 20 March 2015)

Quantization of spin-wave excitations necessitates the reconsideration of the classical fluctuation-dissipation relation (FDR) used for temperature control in spin-lattice dynamics simulations of ferromagnetic metals. In this paper, Bose-Einstein statistics is used to reinterpret the Langevin dynamics of both lattice and spins, allowing quantum statistics to be mimicked in canonical molecular dynamics simulations. The resulting quantum heat baths are tested by calculating the specific heats and magnetization over a wide temperature range, from 0 K to above the Curie temperature, with molecular dynamics (MD), spin dynamics (SD), and spin-lattice dynamics (SLD) simulations. The results are verified with experimental data and available theoretical analysis. Comparison with classical results also shows the importance of quantization effects for spin excitations in all the ferromagnetically ordered configurations.

DOI: 10.1103/PhysRevB.91.104306 PACS number(s): 75.10.−b, 02.70.Ns, 62.20.−x, 75.50.Bb

I. INTRODUCTION

Atomistic modeling provides an important source of information for understanding the behavior of metals and alloys. In applications involving extensive spatial degrees of freedom, in which thermodynamic contributions from low-energy and long-wavelength vibration modes are important, or where lattice defects, correlated dynamics, and critical phenomena are involved, large-scale molecular dynamics (MD) simulations provide the most practical treatment.

In magnetic metals and alloys such as ferritic-martensitic steels, spin polarization is not only responsible for the observed magnetic character, but it also influences many properties of the atomic lattice, such as the type of crystal structure [1], thermal expansivity [2], elastic constants [3], and vacancy formation and migration energy and entropy [4]. Conventional MD simulations omit spin dynamics and hence prevent heat exchange between the lattice and spin subsystems for thermodynamic consideration at finite temperatures. To treat the coupled spin and lattice dynamics in ferromagnetic metals, Ma, Woo, and Dudarev [5,6] (MWD) generalized the MD methodology and developed spin-lattice dynamics (SLD) in which atoms and spins interact through the Heisenberg Hamiltonian with coordinate-dependent exchange parameters. Temperature control is based on the fluctuation-dissipation theorem derived from the Boltzmann statistics neglecting quantization effects [7].

In conventional MD simulations, two assumptions are implicitly made: (1) the validity of the classical particle picture in the definition of phase-space trajectories, and (2) that the vibration energy spectrum is quasicontinuous. The first constraint ensures that quantum tunneling is not important to activation processes, and the second one justifies the use of classical statistics. In this paper, we assume that condition (1) is satisfied. To overcome restriction (2), quantization of vibration energy spectra must be observed, which requires the use of Bose-Einstein statistics in the definition of temperature.

Einstein was the first to consider the effect of quantization on thermal excitations of the crystal lattice in resolving the problem of low-temperature specific heat in classical physics [8]. While phonon excitation is allowed at all temperatures when the phonon energy spectrum is quasicontinuous, this is not so if energy levels are discrete. In Einstein's model, phonon excitations in bcc iron become increasingly difficult below 360 K, because the thermal energy of ∼30 meV required to excite an average phonon is not available. This limits the applicability of Boltzmann statistics to above ∼360 K. The situation is similar in the spin case, but the constraint is more serious. Using the experimental spin stiffness of iron from Collins *et al.* [9] and Mook and Nicklow [10], or the magnon densities of states (DOS) calculated from first principles, excitation of a magnon mode requires a large energy of ∼250–350 meV. As a result, to ensure proper temperature control of SLD simulations below 3000 K, quantization must be taken into account.

In the case of atomic vibrations, Ceriotti *et al.* [11] and Dammak *et al.* [12] demonstrated that by using a generalized Langevin bath with a frequency-dependent (colored) noise, which has been adjusted to produce the characteristic quantum distribution of kinetic energy of simple-harmonic oscillators, quantum statistics may be mimicked in MD simulations. However, a similar scheme suitable for treating spin dynamics is frustrated by the nonparticle-type Hamiltonian. Indeed, treatment of the frequency shift due to magnon softening near the $\alpha-\beta$ (ferro-/paramagnetic) transition temperature [4] is a challenge within the framework of this approach.

In this paper, we aim to reestablish the fluctuation-dissipation relation (FDR) that MWD used to control temperature in SLD by taking into account quantization of phonons and magnons. We follow the route taken by MWD [6], starting with the solution of the Langevin equation that describes the dynamics of a system in a noisy environment in which fluctuating forces and dissipative drag coefficients are characterized by a given fluctuation-dissipation ratio. Quantum fluctuation-dissipation relations (QFDR) for both the lattice and spin systems can then be derived via Bose-Einstein statistics. Adopting the quasiharmonic approximation and

*Corresponding author: chungwoo@cityu.edu.hk

expressing the frequency dependence in terms of temperature-dependent DOS, convenient expressions of the QFDR can be derived for both phonons and magnons. The relevant theoretical background is first reviewed in Sec. II. Quantum FDR for the lattice and spin temperatures are derived in Secs. III and IV, respectively. Simplified models for the temperature-dependent DOS of the quasiharmonic phonons and magnons are suggested in Sec. V. The corresponding heat baths are tested using MD, spin dynamics (SD), and SLD simulations in Sec. VI. In Sec. VII, the simulation results are compared and discussed. Conclusions are given in Sec. VIII.

II. THEORETICAL BACKGROUND

A. Spin-lattice dynamics in a noisy environment

We consider a ferromagnetic metal modeled as a canonical ensemble at temperature T of interacting particles and Heisenberg spin excitations in a noisy environment. Following MWD, the corresponding SLD Hamiltonian can be written as

$$H_{\mathrm{SLD}} = \sum_n \frac{\mathbf{p}_n^2}{2m_n} + U(\{\mathbf{r}\}) - \frac{1}{2}\sum_{n\neq m} J_{nm}(\{\mathbf{r}\})\, \boldsymbol{S}_n \cdot \boldsymbol{S}_m + H_{\mathrm{env}}(T), \qquad (1)$$

where m_n, $\mathbf{p}_n$, and $\mathbf{r}_n$, respectively, are the mass, momentum, and position of the nth atom, and $U(\{\mathbf{r}\})$ is the interatomic potential (many-body) corresponding to the lattice configuration $\{\mathbf{r}\}$, consisting of the ionic Coulomb interaction and contributions from electrons in the ground state. Thus when considering the dynamics of the crystal, the nuclei may be considered to interact via an electronic distribution that depends on the local configuration of the nuclei. The first two terms constitute the Hamiltonian of the system of lattice atoms, describing their statics and dynamics. The third term is the Heisenberg Hamiltonian, representing the spin system in terms of its dynamic states, i.e., magnons. Here $J_{nm}(\{\mathbf{r}\})$ is the exchange interaction function, mainly determined by the overlapping of wave functions of the d electrons, which depends on the atomic distance between the interacting spin pair. $\boldsymbol{S}_n$ is the atomic spin vector (spins in the rest of the current paper) of the nth atom arising from the spin polarization of the atoms according to Hund's rule and is related to its net magnetic moment by $\mathbf{M}_n = -g\mu_{\mathrm{B}}\boldsymbol{S}_n$, where $g(\approx 2)$ is the electronic g factor, μ_{B} the Bohr magneton, and $\boldsymbol{S}_n$ is the atomic spin vector.

In Eq. (1), H_{env} represents the interaction between the Heisenberg subsystem and the heat bath. Via H_{env}, the mechanical system described by Eq. (1) emulates the thermodynamics of a canonical SLD system. H_{env} is also needed to facilitate exchange of energy and angular momentum, without which conservation of the total angular momentum in H_{SLD} prevents full relaxation, constraining a SLD microcanonical ensemble from accessing the lowest free-energy state of thermodynamic equilibrium. This problem has been discussed in detail by MWD [6]. To facilitate the exchange of energy and angular momentum with the environment during equilibration, MWD introduced a noisy environment in which random forces are applied to each atom and spin to emulate the action of a heat bath. Given the fluctuation-dissipation ratio of the noise, the stochastic equations of motion of the atoms and spins consistent with the SLD Hamiltonian in Eq. (1) can be derived [6]. The canonical thermodynamics of the system is then obtained via a relation that links the fluctuation-dissipation ratio to the temperature. This relation is the classical fluctuation-dissipation theorem derived based on the assumption that the dynamical states, i.e., phonons and magnons, have energies that are continuously distributed according to Boltzmann statistics [13]. To consider quantization effects in the fluctuation-dissipation relation, which is the main task of this paper, quantum statistics will have to be used in the description of the elementary thermal excitations.

B. Temperature-dependent phonons and magnons

The temperature of a canonical ensemble is intimately related to the statistical thermodynamics of its thermal excited states. Thermal excitations in ferromagnetic metallic crystals are predominantly in the form of elastic and spin waves, i.e., correlated lattice and spin vibrations. When the vibrations are harmonic, statistical thermodynamics can be readily treated via Bose-Einstein statistics [14]. However, thermal vibrations in real solids are anharmonic in general, with amplitude-dependent restoring forces.

To treat this problem, the concept of temperature-dependent phonon (magnon) states is useful. In this regard, a crystal Hamiltonian H can generally be expressed as the sum of a harmonic component H_h and an anharmonic correction $\Delta_a \equiv H\text{-}H_h$. In terms of the complete orthonormal set of eigenstates $\{|n,\mathbf{k}\rangle\}$ of H_h, H can be represented by the matrix elements

$$\langle m,\mathbf{k}'|H|n,\mathbf{k}\rangle = \{(n+1/2)\hbar\omega_k + \langle n,\mathbf{k}|\Delta_a|n,\mathbf{k}\rangle\}\delta_{mn}\delta_{\mathbf{k}\mathbf{k}'} + \langle m,\mathbf{k}'|\Delta_a|n,\mathbf{k}\rangle_{m\neq n,\mathbf{k}\neq\mathbf{k}'}, \qquad (2)$$

where ω_k is the phonon (magnon) frequency, and $\boldsymbol{k}$ is the wave vector. The diagonal elements given by the term in curly brackets represent phonon (magnon) states of the kth mode, and the off-diagonal elements in the last term account for the mixing of the phonon (magnon) states due to anharmonicity. According to Eq. (2), Δ_a produces two effects: (1) phonon (magnon) frequency shift and (2) line broadening via phonon (magnon) scattering. The former corresponds to a first-order perturbation correction, and the latter, second- and higher-order corrections. It is important to note that at this point H_h is arbitrary and the corresponding phonon (magnon) description is not unique. Using a harmonic crystal potential in H_h which minimizes the off-diagonal elements is obviously desirable. The common practice is to define the harmonic Hamiltonian $H_h(0)$ with a stiffness based on the 0-K (ground-state) crystal properties such as elastic modulus, lattice constants, magnetization, etc. and neglect the off-diagonal elements for low-temperature small-amplitude vibrations. The corresponding "0-K" phonon (magnon) states can then be substituted for the eigenstates of H in the thermodynamic description of the low-temperature thermal excitations. In view of the amplitude dependence of the stiffness, the use of "0-K" phonons (magnons) for a finite-temperature representation of H is not the only choice and is by no means the most suitable. Instead, by constructing $H_h(T)$ with a stiffness suitable for temperature T and the corresponding off-diagonal elements neglected as higher-order corrections, H in Eq. (2) is expressible

as an explicitly temperature-dependent phonon (magnon) Hamiltonian: $H \simeq \sum_{\mathbf{k},n} (n+1/2)\hbar\omega_k(T)|n,\mathbf{k}\rangle\langle n,\mathbf{k}|$. Here anharmonic frequency shift has been taken into account in $\omega_k(T)$. In this representation, the eigenstates of H can be approximated by the phonon (magnon) states $|n,\mathbf{k}\rangle$ with eigenvalues $(n+1/2)\hbar\omega_k(T)$, to which the Bose-Einstein statistics can be used in deriving the fluctuation-dissipation relation for the emulating noise in the Langevin heat bath. Given the emulating noise, an SLD simulation is carried out with the full (i.e., not harmonized) interatomic and magnetic interactions in $H_{\rm SLD}$ in Eq. (1).

Indeed, the concept of temperature-dependent phonons is not new. The subject has been elucidated in many standard solid-state physics textbooks (see, for example, [15]) under the term quasiharmonic approximation for considering the thermodynamics of lattice vibrations at finite temperature. Its application in the treatment of anharmonicity has also been discussed by Fultz [14] in his celebrated review of vibrational thermodynamics. For the same purpose, temperature-dependent magnons can also be similarly defined based on the dispersion relation and DOS from the temperature-dependent spin stiffness.

The use of the temperature-dependent phonon and magnon representations goes a long way in improving the accuracy of the temperature-dependent frequency distribution due to the anharmonic shift and helps minimize the phonon (magnon) line broadening due to the nondiagonal matrix elements. It is helpful that remaining errors are further reduced because quantization and anharmonic effects on the statistics are rarely important in the same temperature regime. Indeed, at low temperatures, where quantization effects in the statistical distribution are important [$\hbar\omega_k(T) \gg k_{\rm B}T$], vibration amplitudes are small and anharmonic effects are expected to be weak. On the other hand, at high temperatures, where large vibration amplitudes produce large anharmonic effects, phonon and magnon energy spectra may be considered quasicontinuous [$\hbar\omega_k(T) \ll k_{\rm B}T$], and classical thermodynamics apply, which is insensitive to the frequency distribution. Thus, within the present context, where the focus is the fluctuation-dissipation relation for the heat bath, the use of temperature-dependent frequency distributions within the quasiharmonic scheme could be considered adequate.

III. QFDR FOR LATTICE SYSTEM

Let us first consider the relation between the fluctuation-dissipation ratio and the temperature in the lattice system. At a fixed temperature T, the lattice part of the Hamiltonian constitutes the first two terms of $H_{\rm SLD}$ in Eq. (1). In terms of the Cartesian components with subscripts $i(=x,y,z)$, it can be expressed as

$$H_L(\{r_{ni}\},\{p_{ni}\}) = \sum_{n,i} \frac{p_{ni}^2}{2m_n} + U(\{r_{ni}\}). \tag{3}$$

Under the action of frequency-independent δ-correlated random forces $\mathbf{f}_n(t)$ in $H_{\rm env}(T)$, defined by

$$\langle \mathbf{f}_n(t)\rangle = 0 \quad \text{and} \quad \langle f_{in}(t) f_{jl}(t')\rangle = \mu_L(T)\delta_{ij}\delta_{nl}\delta(t-t'), \tag{4}$$

the classical equations of motion of the ith Cartesian component of the nth particles can be written as

$$\begin{cases} \dfrac{dr_{ni}}{dt} = \dfrac{\partial H_L}{\partial p_{ni}} = \dfrac{p_{ni}}{m_n}, \\ \dfrac{dp_{ni}}{dt} = -\dfrac{\partial H_L}{\partial r_{ni}} - \dfrac{\gamma_L}{m_n} p_{ni} + f_{ni}(t) = -\dfrac{\partial U}{\partial r_{ni}} - \dfrac{\gamma_L}{m_n} p_{ni} + f_{ni}(t) \end{cases}, \tag{5}$$

where $-\gamma_L(T)\mathbf{p}_n/m_n$ is the viscous drag on the motion of the nth particle due to the random forces. We characterize the Langevin bath by the fluctuation-dissipation ratio $\eta_L(T) \equiv \mu_L/2\gamma_L$. The corresponding phase-space probability density $W(\{r_{ni}\},\{p_{ni}\},t)$ is governed by the corresponding Fokker-Planck equation [13]:

$$\sum_{n,i} \left\{ \frac{\partial}{\partial t} + \frac{p_{ni}}{m_n}\frac{\partial}{\partial r_{ni}} - \left(\frac{\partial U}{\partial r_{ni}}\right)\frac{\partial}{\partial p_{ni}} \right\} W = \sum_{n,i} \frac{\partial}{\partial p_{ni}} \left[\gamma_L \frac{p_{ni}}{m_n} + \frac{\mu_L}{2}\frac{\partial}{\partial p_{ni}} \right] W. \tag{6}$$

At steady state, $W(\{r_{ni}\},\{p_{ni}\},t)$ is time independent and $\partial W/\partial t = 0$. In this case, Eq. (6) can be solved with a trial function of the form $W^\infty = C\exp(-\beta_L H_L)$, where β_L is an unknown coefficient to be determined and C is a normalizing constant. Substituting W^∞ into Eq. (6), we obtain

$$\gamma_L \sum_{n,i} \frac{p_{ni}}{m_n} (1 - \beta_L\eta_L) W^\infty = 0, \tag{7}$$

with the solution $\beta_L^{-1} = \eta_L$, and the corresponding phase-space probability density at temperature T can be written as

$$W^\infty(\{r_{ni}\},\{p_{ni}\}) = C\exp\left[-\frac{H_L}{\eta_L}\right]. \tag{8}$$

The ensemble-averaged kinetic energy of the dynamical system can be directly evaluated using the phase-space probability distribution in Eq. (8), yielding

$$\sum_{ni} \left\langle \frac{p_{ni}^2}{2m_n} \right\rangle = \langle E_K\rangle = \frac{3N\eta_L}{2}. \tag{9}$$

Equation (8) is valid independent of the crystal potential $U(\{r_{ni}\})$ experienced by the atoms, which is independent of $\{p_{ni}\}$. In other words, one may remove the nonharmonic part of U without affecting Eq. (9). We note in passing that Eq. (9) can also be derived directly from the Langevin equation, i.e., Eq. (5), without having to go through the Fokker-Planck equation [6].

If a *continuous* vibration spectrum is assumed, the corresponding average kinetic energy $\langle E_K\rangle_c = \frac{3}{2}Nk_{\rm B}T$ can be obtained by integrating with the Boltzmann distribution, with $k_{\rm B}$ being Boltzmann's constant. The corresponding relation between the fluctuation-dissipation ratio $\eta_L(T)$ and the thermodynamic temperature T then follows from Eq. (9) and takes the form of the classical fluctuation-dissipation theorem (FDT), $\eta_L(T) = k_{\rm B}T$ [13].

Energy quantization, however, dictates that with the use of quantum statistics for the equilibrium energy distribution Eq. (9) does not give the classical equipartition theorem, which

is the base of the classical FDT that MWD used previously to bridge mechanics and thermodynamics. To reestablish this connection, $\langle E_K \rangle$ in Eq. (9) must be equated to $\langle E_K \rangle_q$ calculated quantum mechanically.

Within the quasiharmonic approximation, we may apply the quantum virial theorem [16] and equate $\langle E_K \rangle_q$ to half of the total temperature-dependent phonon energy. Thus

$$\langle E_K \rangle_q = \frac{1}{2} \sum_{\boldsymbol{k}} \sum_{\alpha=1}^{3} \hbar\omega_\alpha(\boldsymbol{k}) \left[\frac{1}{e^{\hbar\omega_\alpha(\mathbf{k})/k_\mathrm{B}T} - 1} + \frac{1}{2} \right], \quad (10)$$

where $\hbar$ is the Planck's constant. We note that the phonon energy spectrum $\hbar\omega_\alpha(\boldsymbol{k})$ is a function of temperature-dependent properties of the crystal lattice (see Sec. II B). Equating $\langle E_K \rangle_q$ in Eq. (10) with $\langle E_K \rangle$ in Eq. (9), we obtain a nonlinear QFDR given by

$$\eta_L(T) = \frac{1}{3N} \sum_{\boldsymbol{k}} \sum_{\alpha=1}^{3} \hbar\omega_\alpha(\boldsymbol{k}) \left[\frac{1}{e^{\hbar\omega_\alpha(\boldsymbol{k})/k_\mathrm{B}T} - 1} + \frac{1}{2} \right] = \int_0^\infty \hbar\omega \left[\frac{1}{e^{\hbar\omega/k_\mathrm{B}T} - 1} + \frac{1}{2} \right] g_p(\omega, T)\, d\omega. \quad (11)$$

We note that the QFDR in Eq. (11) is completely determined by the phonon density of states ($p-$DOS) at T, $g_p(\omega,T) = \frac{4\pi k^2 \Omega}{(2\pi)^3} [\nabla_{\boldsymbol{k}} \omega(T)]^{-1}$ [15], where Ω is the atomic volume. As discussed in Sec. II B, the $p-$DOS is a function of the crystal structure and force constants, both of which are temperature dependent. Thus, given temperature T, canonical MD simulations can be performed using Langevin forces defined by the fluctuation-dissipation ratio $\eta_L(T)$ according to Eq. (11).

In Eq. (11), the contribution associated with the first term in the square bracket accounts for the thermal fluctuations due to phonons, while the second term represents the zero-point fluctuations due to the uncertainty principle. Fluctuations due to this contribution have a quantum origin and are present even at 0 K when phonons are absent. This is in contrast to the classical formulation of MWD, in which fluctuations are completely absent at 0 K.

The dependence of the QFDR on the $p-$DOS in Eq. (11) can be traced to the frequency dependency of the random forces that emulate the quantum heat bath [11,12]. Thus, despite the white-noise appearance of the associated Langevin bath considered here, it is in reality an alternate form of the color-noise scheme. In this form, physical transparency allows the use of simplifying approximations for the DOS, which is particularly important when spin dynamics is considered in later sections.

IV. QFDR FOR THE SPIN SYSTEM

The procedure developed for the lattice system can now be adapted to the spin system. A generic Heisenberg Hamiltonian describing a broad class of spin systems in the absence of an external field can be written in the form [17]

$$H_S \equiv -\frac{1}{2} \sum_{\substack{n,m \\ m \neq n}} J_{nm} \boldsymbol{S}_n \cdot \boldsymbol{S}_m. \quad (12)$$

We model spin interaction with the noisy environment in the same way as MWD: by the action of white noise $\mathbf{h}_n(t)$ defined by $\langle \boldsymbol{h}_n(t) \rangle = 0$ and $\langle h_{ni}(t) h_{mj}(t') \rangle = \mu_S \delta_{nm} \delta_{ij} \delta(t - t')$. Similar to the lattice case, μ_S is a parameter characterizing the amplitude of the random field, γ_S is the corresponding dissipative drag coefficient, and i and j denote the Cartesian components of a vector. We also characterize the Langevin bath using the fluctuation-dissipation ratio $\eta_S \equiv \mu_S / 2\hbar\gamma_S$, as in MWD. Dropping the subscript n for convenience, the equation of motion for the nth spin can be expressed as the following stochastic differential equation:

$$\frac{d\boldsymbol{S}}{dt} = \frac{1}{\hbar} [\boldsymbol{S} \times (\boldsymbol{H} + \boldsymbol{h}(t)) - \gamma_S \boldsymbol{S} \times (\boldsymbol{S} \times \boldsymbol{H})], \quad (13)$$

where the effective field $\boldsymbol{H}$ acts on the spin. The corresponding Fokker-Planck equation can be established following the Appendix of [7]. Similar to the lattice case treated in the foregoing section, the equilibrium phase-space probability distribution function of the spin system W_S^e can be obtained from the steady-state Fokker-Planck equation (i.e., with $\partial W_S / \partial t = 0$) by using the trial function $W_S^e = C \exp(-\beta_S H_S)$, where β_S is an unknown coefficient to be determined and C is a normalization constant. Proceeding similar to [7], we obtain

$$\beta_S^{-1} = \eta_S, \quad (14)$$

and, consequently,

$$W_S^e(\{\boldsymbol{S}_n\}) = C \exp\left(-\frac{H_S}{\eta_S} \right). \quad (15)$$

Similar to the phonon case, it is clear that this equation reproduces the Boltzmann distribution with $T = \eta_S / k_\mathrm{B}$ [7], if quantization can be neglected.

Taking energy quantization into account with the Bose-Einstein distribution leads to a more complex relation between T and η_S. To derive the QFDR for a spin system at a specific temperature T, we consider the case of a crystal with N atoms arranged in a crystal lattice specific to T. Following Ref. [18] and designating the spin of the nth atom by $\boldsymbol{S}_n$, the Heisenberg Hamiltonian in Eq. (12) can be written in the second-quantized form (via the Holstein-Primakoff [18] mapping) as

$$H_S(\{\boldsymbol{S}_n\}) = -\frac{1}{2} N H_0 S + \sum_k \hbar\omega_k b_k^+ b_k + H_{mm}, \quad (16)$$

where $\boldsymbol{H}_0$ is the effective field $\boldsymbol{H}$ with collinear spins, $n_k = b_k^+ b_k$ is the occupation number, and ω_k is the frequency of k-mode magnons at temperature T under consideration (see Sec. II B). We emphasize that the magnon state considered here is specific to the spin stiffness at T. It is different from $n_k(0)$ and $\omega_k(0)$ based on the 0-K spin stiffness usually considered. Indeed, this difference applies to both $n_k(T)$ and $\omega_k(T)$, and thus also to the dispersion relation and DOS. The temperature dependence of the vibration frequencies can also be seen via the effective field in Eq. (13).

In Eq. (16) the first two terms constitute the magnon Hamiltonian [19] and the last term H_{mm} represents the nondiagonal anharmonic matrix elements discussed at length in Sec. II B. Within the quasiharmonic approximation of finite-temperature magnons, we may neglect H_{mm}. Thus, contrary to the 0-K magnons, finite-temperature magnons can be assumed

to be noninteracting at T and the spin system in Eq. (16) can be considered as $3N$ independent quasiharmonic oscillators. The Bose-Einstein ensemble average of the total energy then follows from Eq. (16):

$$\langle E\rangle = \langle H_S\rangle = -\frac{1}{2}NH_0S + \sum_k \langle n_k(T)\rangle \hbar\omega_k$$
$$= -\frac{1}{2}NH_0S + \sum_k \frac{\hbar\omega_k(T)}{\exp\left[\hbar\omega_k(T)/k_BT\right]-1}. \quad (17)$$

On the other hand, the quasiharmonic mean energy of the ensemble of spins at T interacting with the noisy environment is given by (see Appendix)

$$\langle E\rangle = N\eta_S - \tfrac{1}{2}NH_0S. \quad (18)$$

Equating Eqs. (17) and (18) yields the QFDR for a spin system:

$$\eta_S(T) = \frac{1}{N}\sum_k \frac{\hbar\omega_k}{\exp\left(\hbar\omega_k/k_BT-1\right)}$$
$$= \int_0^\infty \frac{\hbar\omega}{\exp\left(\hbar\omega/k_BT\right)-1} g_m(\omega,T)\,d\omega. \quad (19)$$

Here $g_m(\omega,T)$ is the magnon density of states ($m-$DOS) at temperature T. Similar to the $p-$DOS, the $m-$DOS $g_m(\omega,T) \equiv \frac{\Omega}{(2\pi)^3}\cdot\frac{4\pi k^2}{\nabla_k\omega(T)}$ is a function of temperature. Given temperature T, spin-dynamics calculations can therefore be carried out using Langevin forces defined by the fluctuation-dissipation ratio $\eta_S(T)$ according to Eq. (19). We note that the QFDRs in Eqs. (11) and (19) are the main results of this paper.

The $m-$DOS can be obtained from experiments, from first-principle calculations, or by using a simplified model based on the quasiharmonic approximation, as discussed in the following section. Similar to the phonons, the influence of temperature dependence has to be considered in the calculation of the $m-$DOS.

V. SIMPLE ANALYTICAL MODELS FOR THE DOS

One may observe that the integrants in Eqs. (11) and (19) are heavily weighted towards the low-frequency long-wavelength excitations, except at high temperatures, in which case all vibration modes are excited irrespective of frequency, and the details of the frequency dependence are no longer important, resulting in the disappearance of quantization effects. This observation suggests simple approximations of the DOS that can be used in evaluating the QFDR for both phonons and magnons.

A. Test of QFDR using the Debye model for the lattice system

The Debye model is well known to give the correct thermodynamics of many nonmagnetic crystals in both low- and high-temperature limits. Within the Debye model [15], the $p-$DOS for calculating the QFDR in Eq. (11) can be written as

$$g_p(\omega) = \begin{cases} \frac{\Omega}{2\pi^2 c_s^3}\omega^2 & \text{for} \quad \omega \leqslant \omega_D \\ 0 & \text{for} \quad \omega > \omega_D \end{cases}, \quad (20)$$

where c_s is the temperature-dependent effective sound speed (mean lattice-wave group velocity) and $\omega_D = \left(\frac{6\pi^2}{\Omega}\right)^{1/3} c_s$ is the Debye frequency that marks the phonon spectral limit, both of which can be linearly expressed in terms of the Debye temperature Θ_D according to $k_B\Theta_D = \hbar\omega_D$. We note that Θ_D uniquely specifies the $p-$DOS and follows the temperature dependence of c_s.

Substituting Eq. (20) into Eq. (11), the QFDR is given in terms of the Debye temperature by

$$\eta_L(T) = \frac{3}{8}k_B\Theta_D + 3k_B\Theta_D\left(\frac{T}{\Theta_D}\right)^4 \int_0^{\frac{\Theta_D}{T}} \frac{x^3}{e^x-1}\,dx, \quad (21)$$

which expresses the QFDR for a lattice system in the Debye model. In the classical limit, Θ_D/T goes to zero, and the corresponding QFDR obtained from Eq. (21) yields the classical fluctuation-dissipation theorem $\eta_L = k_BT$.

As a test of the simplified QFDR in the foregoing, we apply it to a harmonic lattice model. In this case, the thermal energy can be expressed by solving the corresponding stochastic equation of motion in Sec. III, yielding $\langle E\rangle = 3N\eta_L$. The heat capacity of the Debye crystal can be obtained according to

$$C_p(T) = \frac{d\langle E\rangle}{dT} = 9Nk_B\left(\frac{\Theta_D}{T}\right)^{-3}\int_0^{\frac{\Theta_D}{T}} \frac{x^4e^x}{(e^x-1)^2}\,dx$$
$$\equiv 3Nk_Bf_D\left(\frac{\Theta_D}{T}\right), \quad (22)$$

where f_D is the Debye function [20]. Equation (22) is precisely the same well-known expression for heat capacities that can be derived within the Debye model directly from quantum statistics [20]. From Eq. (22), other thermodynamic quantities, such as the entropy, free energy, heat conductance, etc., can be expressed in the harmonic approximation as a function of Θ_D/T. The low- and high-temperature limits of Eq. (22) are given by the well-known expressions

$$C_p(T) = \begin{cases} \frac{12\pi^4Nk_B}{5}\left(\frac{T}{\Theta_D}\right)^3 & \text{for} \quad T \ll \Theta_D \\ 3Nk_B & \text{for} \quad T \gg \Theta_D \end{cases}. \quad (23)$$

Equations (22) and (23) verify the methodology adopted in deriving Eq. (11).

Although anharmonicity of the crystal potential does not affect the mean kinetic energy of the lattice system which defines its temperature [see Eq. (9)], the temperature dependences of other thermodynamic functions, such as the mean total energy, heat capacity, entropy, and free energy, depend on the potential energy and are thus affected by its anharmonicity. If we put $\langle E_k\rangle = \frac{1}{2}\langle E_h\rangle$, where E_h is the total energy in the harmonic approximation, the energy correction due to anharmonicity can be measured by a parameter α_{ah}^L, where

$$\alpha_{ah}^L = \frac{\langle E\rangle}{\langle E_h\rangle} = \frac{\langle E\rangle}{3N\eta_L}. \quad (24)$$

Therefore, at high temperatures, $\langle E\rangle = \alpha_{ah}^L\langle E_h\rangle = 3N\alpha_{ah}^Lk_BT$.

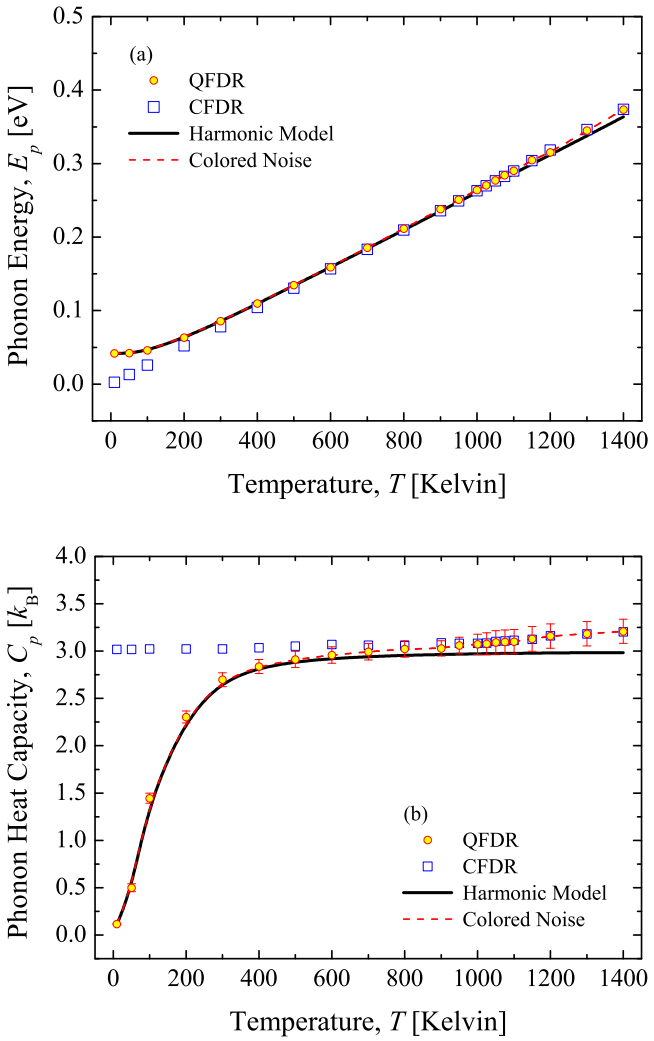

FIG. 1. (Color online) (a) The thermal energies E_p and (b) the specific heat C_p due to lattice vibrations computed by MD simulations using quantum (blue open squares, QFDR) and classical (red open circles, CFDR) fluctuation-dissipation relation schemes. Results from the 0-K harmonic model [see Eqs. (10) and (23), black solid line] and colored-noise scheme [12,29] are also presented for comparison.

A fully anharmonic calculation of phonon thermal energy $E_p(T)$ and heat capacity $C_p(T)$ of bcc iron in which the ensemble energy is obtained from MD with the Dudarev-Derlet (DD) potential yields results shown in Figs. 1(a) and 1(b). Plotted for comparison in the same figure are results for bcc iron calculated with the quantum color-noise bath as well from Eq. (23). The results from our white-noise and color-noise baths are practically identical and agree very well with Eq. (22) at low temperatures, as they should. At higher temperatures, the difference between the harmonic and the MD models reflects the quasiharmonic contributions. Details of the calculation are further discussed in Sec. VII A.

B. Test of QFDR in a low-temperature analytic model for magnons

As discussed in Sec. II B, the anharmonic contribution H_{mm} in Eq. (16) is neglected within the quasiharmonic approximation. In this section, we concentrate on the low-temperature case, where high-energy and high-k vibration modes can be neglected such that an analytic QFDR is derivable. At low temperatures, the dynamical state of the corresponding spin ensemble can be represented by low-k magnons with a dispersion relation given by $\hbar\omega = D_0 k^2$ [17]. The $m-$DOS $g_m(\omega) \equiv \frac{\Omega}{(2\pi)^3} \cdot \frac{4\pi k^2}{\nabla_k \omega}$ can be described similar to the lattice case by a Debye-like model [17] with the following form:

$$g_m^h(\omega) = \begin{cases} \frac{\Omega}{4\pi^2}\left(\frac{\hbar}{D_0}\right)^{3/2}\omega^{1/2} & \text{for} \quad \omega \leqslant \omega_h \\ 0 & \text{for} \quad \omega > \omega_h \end{cases}. \tag{25}$$

We may call $g_m^h(\omega)$ in Eq. (25) the harmonic $m-$DOS, where D_0 is the ground-state spin stiffness, $\Omega = a^3/2$ is the atomic volume evaluated at ground state in a bcc structure with lattice constant a, and ω_h is the corresponding cutoff frequency defined by the normalizing condition $\int_0^{\omega_h} g_m^h(\omega)d\omega = 1$. The corresponding cutoff temperature $\Theta_h = \hbar\omega_h/k_B$ is related to D_0 through Eq. (25) according to

$$\Theta_h = \frac{D_0}{k_B}\left(\frac{6\pi^2}{\Omega}\right)^{2/3}. \tag{26}$$

For bcc iron, with an estimated $a \approx 0.287$ nm and $D_0 \approx 3.50 \times 10^{-3}$eV nm^2 [9,10], Eq. (26) gives a value for Θ_h of 11 892 K, which is very much higher than the Debye temperature for phonons ($\Theta_D = 470$ K for iron), and also the experimental Curie temperature ($T_C = 1043$ K). With $g_m^h(\omega)$ given by Eq. (25), the QFDR in Eq. (19) can be expressed analytically in terms of Θ_h as

$$\eta_S(T) = \frac{3}{2}k_B\Theta_h\left(\frac{T}{\Theta_h}\right)^{5/2}\int_0^{\frac{\Theta_h}{T}}\frac{x^{3/2}}{e^x-1}\,dx. \tag{27}$$

Comparing Eqs. (21) and (27), it is clear that spin and lattice systems have different fluctuation-dissipation ratios, unless their temperatures are much higher than both Θ_h and Θ_D when $\eta_L = \eta_S = k_B T$.

Similar to the phonon case, an analytic expression for the heat capacity in the low-temperature approximation can be derived by applying the QFDR in Eq. (27) to the stochastic equation of motion in Sec. IV. Equation (18) gives

$$C_m(T) = \frac{d\langle E\rangle}{dT} = \frac{d\eta_S}{dT} = Nk_B f_m\left(\frac{\Theta_h}{T}\right), \tag{28}$$

where f_m is defined by

$$f_m(y) \equiv \frac{3}{2}y^{-3/2}\int_0^y \frac{e^x x^{5/2}}{(e^x-1)^2}\,dx, \tag{29}$$

with high- and low-temperature limits given by

$$C_m^h(T) = \begin{cases} 0.113Nk_B\frac{\Omega}{a^3}\left(\frac{k_B T}{D_0/a^2}\right)^{3/2} & \text{for} \quad T \ll \Theta_h \\ Nk_B & \text{for} \quad T \gg \Theta_h \end{cases}. \tag{30}$$

The heat capacity in Eq. (30) is precisely the same as that obtained directly from quantum mechanics using the low-k quadratic dispersion relation [19]. Other thermodynamic

quantities such as the entropy, free energy, and heat capacity can also be calculated from the heat conductance as a function of T, similar to the phonon case. Equations (28)–(30) verify the methodology adopted in deriving Eq. (19).

C. Simplified model of DOS for magnons at higher temperature

As pointed out in Sec. II B, the low-k approximation in Sec. V B is not useful for the $m-$DOS at higher temperatures. At the same time, effects on the $m-$DOS due to the strong temperature dependence of the effective field that drives the spin dynamics must also be accounted for, particularly near the Curie temperature. The corresponding treatment of the $m-$DOS will be discussed in the following two sections. We first consider relaxing the low-k approximation. The treatment of magnon softening will then follow.

1. Correcting the low-k assumption

Comparing with *ab initio* results [21] at 0 K [see Fig. 2(a)], it can be seen that the harmonic $m-$DOS in Eq. (25) is valid only for energy levels below 200 meV. Over 80% of the magnon energy levels are much overestimated. This large error in the frequency distribution is likely due to the loss of the Van Hove singularity in the low-k approximation for the magnon dispersion relation. To include contributions from vibration modes with higher k, we expand the magnon dispersion relation up to the quartic power, i.e.,

$$\hbar\omega = Dk^2(1 - bk^2), \tag{31}$$

where b is a fitting parameter to give the correct singularity at $k = 1/\sqrt{2b}$ where the corresponding magnon group velocity is zero. Expressing k in terms of ω in Eq. (31), the corresponding $m-$DOS can be derived similar to Eq. (25):

$$g_m^b(\omega,T) = \begin{cases} \dfrac{\hbar\Omega}{4\pi^2 D(T)} \cdot \dfrac{\sqrt{\frac{1}{2b}\left(1-\sqrt{1-\frac{4\hbar\omega b}{D(T)}}\right)}}{\sqrt{1-\frac{4\hbar\omega b}{D(T)}}} & \text{for} \quad \omega \leqslant \omega_b = \dfrac{D(T)}{4\hbar b} \\ 0 & \text{for} \quad \omega > \omega_b \end{cases}. \tag{32}$$

Here $\omega_b = \frac{D}{4\hbar b}$ is the cutoff frequency. By identifying the pole of Eq. (32) at $k = 1/\sqrt{2b}$ with the Van Hove singularity in the *ab initio* $m-$DOS [21] [see Fig. 2(a)], we obtain a value of $b \approx 2.85 \times 10^{-3}\text{nm}^2$. The normalizing condition can then be satisfied by using a normalizing constant. The resulting $m-$DOS generated from Eq. (32) is shown in Fig. 2(a), together with the *ab initio* results. The corresponding cutoff temperature $\Theta_b = D/4k_B b$ is temperature dependent via the spin stiffness $D(T)$ (see next section). At 0 K, it has a value of 3563 K, much lower than the 11 892 K obtained without the k^4 correction.

D. Temperature dependence of the $m-$DOS

To treat the temperature-dependent magnons in the QFDR, an explicitly temperature-dependent form of the $m-$DOS is needed in Eq. (19). As discussed in Sec. II B, magnon frequency spectra and eigenstates are functions of temperature due to the amplitude-dependent force constant in the spin vibrations. Near the Curie temperature T_C, magnons soften and their frequencies slow down critically to zero as magnetization disappears at the ferro-/paramagnetic transition point. Since the spin stiffness $D(T)$ is directly proportional to the magnetization via the effective field, it can be treated as an order parameter in the Landau theory of phase transition. Its temperature dependence may be written explicitly in the form [22]

$$D(T) = D_0(1 - T/T_C)^{\beta_c}, \tag{33}$$

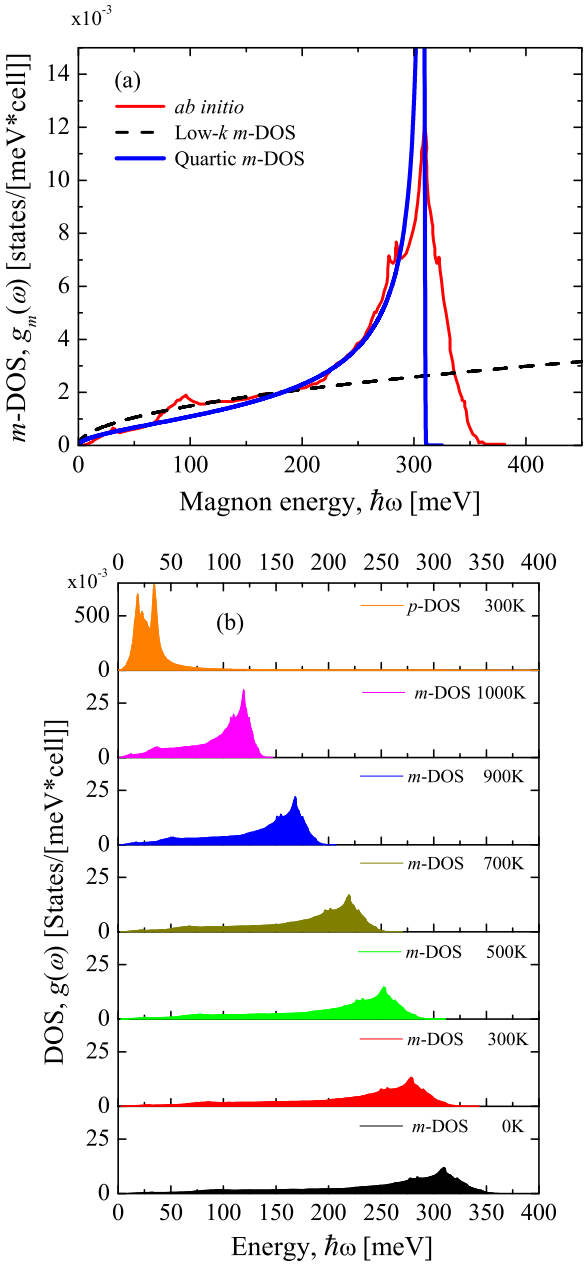

FIG. 2. (Color online) (a) The 0-K magnon density of states ($m-$DOS) in low-k [Eq. (25), black solid line] and quartic approximations [Eq. (32), blue solid line], plotted in comparison with *ab initio* results [21] (red solid line). Note that in the quartic $m-$DOS with $b \approx 2.85 \times 10^{-3}\text{nm}^2$, the Van Hove singularity is well reproduced. (b) The temperature-dependent $m-$DOS according to Eq. (33). The $p-$DOS at 300 K is also plotted for comparison.

where D_0 is the stiffness at 0 K, and β_c is the critical index ($\beta_c = 1/3$ is chosen according to Ref. [23]). Using Eq. (33), the corresponding cutoff frequency $\omega_b = D/4\hbar b$ can be written as an explicit function of temperature:

$$\omega_b = \frac{D_0(1 - T/T_C)^{\beta_c}}{4\hbar b}. \tag{34}$$

When ω_b in Eq. (34) is used in Eq. (32), we have a temperature-dependent quasiharmonic $m-$DOS $g_m^b(\omega, T)$ with a small cutoff frequency at temperatures near T_C. As this happens, the magnon frequency tends to zero and their energy spectrum becomes quasicontinuous. Thus quantum statistics reverts back to classical statistics at temperatures near T_C.

Figure 2(b) demonstrates the anharmonic downshift of the temperature-dependent magnon frequencies, i.e., softening, as the spin system approaches the Curie point. In this figure, the temperature-dependent $m-$DOS are obtained by transforming the 0-K energy distribution from *ab initio* results [21] using Eq. (33). In perspective, the $p-$DOS is also plotted in Fig. 2(b). It can be seen that at low temperatures the phonon frequencies are indeed an order of magnitude smaller than the magnon frequencies. The increasing overlap between the $m-$DOS and $p-$DOS as temperature approaches T_C (=1043 K) is clear, suggesting increasingly coupled magnetic and lattice properties due to the enhancement of phonon-magnon interaction in this temperature range.

The expression for the magnon QFDR in Eq. (19) calculated with the quasiharmonic $m-$DOS according to Eq. (32) with the corresponding ω_b in Eq. (34) and $D(T)$ in Eq. (33) can be used in conventional spin dynamics as well as SLD.

VI. TEST OF QFDR

The QFDRs developed in Eqs. (11) and (19) have been tested in analytic harmonic models in Sec. V. In this section, they are put to the test in fully anharmonic MD, SD, and SLD simulations in bcc iron. The lattice and spin dynamics in the simulations are respectively governed by the nonmagnetic interatomic potential and the Heisenberg-type spin-spin exchange interaction, as shown in Eq. (1). The DD potential [24] $U_{\rm DD}(\mathbf{r})$ is used to describe the interatomic interactions in the magnetic ground state, in which the atomic spins are all collinear. The exchange integral $j_{ij}(\mathbf{r})$ has the form given in Ref. [6],

$$j_{ij}(r_{ij}) = j_0(1 - r_{ij}/r_c)^3\Theta(r_c - r_{ij}), \tag{35}$$

where j_0 is a parameter best fitted to *ab initio* data, and $r_c = 3.75$ Å is the cutoff radius located between the second- and the third-nearest-neighbor distance in bcc iron. $\Theta(x)$ is the Heaviside step function. In Eq. (35), the exchange integral is a pairwise function of the lattice configuration, defined as the product of the exchange integral $J_{ij}(\mathbf{r})$ and the magnitudes of spins S_i and S_j, i.e., $j_{ij}(r_{ij}) = J_{ij}(r_{ij})S_iS_j$. In terms of j_{ij}, the nonmagnetic interatomic potential in Eq. (1) can be written as

$$U(\{\mathbf{r}_i\}) = U_{\rm DD}(\{\mathbf{r}_i\}) - \left\{-\frac{1}{2}\sum_{i\neq j} j_{ij}(r_{ij})\right\}. \tag{36}$$

The potential $U(\{\mathbf{r}_i\})$ describes the nonmagnetic contribution to the bonding energy of ferromagnetic iron in Eq. (1).

The simulation cell contains 16 000 atoms in a box of $20 \times 20 \times 20$ bcc unit cells in the Cartesian coordinate system. Periodic boundary conditions are applied to avoid free surfaces. To allow for magnon softening near T_C [25], at least 2 ns of equilibration time is used. The computation is performed using the Suzuki-Trotter decomposition [26] with a time step of 1 fs.

For lattice dynamics, *NPT* simulations are carried out with the Langevin heat bath based on the QFDR in Eq. (11), using the Berendsen barostat [27] to control the atomic volume under zero pressure. The sampling time is 1 ns after thermal equilibrium. For the QFDR of the lattice in Eq. (11), a Debye model of the $p-$DOS is used with a Debye temperature Θ_D, which is mainly determined by the interatomic potential, set at 430 K [28]. To compare, the quantum color-noise Langevin thermostat is also applied to the lattice system [12,29], where the frequency cutoff $\omega_{\rm max} = 2\pi/\tau$ is set at $\sim 10^{15}$ Hz (τ is the fixed simulation time step, $\tau = 10^{-15}$s). During the simulations, the relaxation and sampling times are both set at 1 ns to minimize statistical error.

For the spin dynamics, NVT simulations are performed with a Langevin heat bath based on the QFDR in Eq. (19). We use the $m-$DOS in Eq. (32) with the temperature-dependent ω_b in Eq. (34). The 0-K spin stiffness D_0 and Curie temperature T_C of the ferromagnetic system are both determined from the exchange interaction according to $D_0 = J_{ij}a^2S$ and $\frac{3}{2}Nk_{\rm B}T_C = \frac{1}{2}\sum_{i,j} J_{ij}S(S+1)$ [18], where J_{ij} is the exchange integral, a is the lattice constant, and S is the magnitude of atomic spin (see Eq. (7.52) in Ref. [18]).

VII. RESULTS AND DISCUSSION

A. Energy and heat capacity of the lattice system from MD simulation

In Figs. 1(a) and 1(b), we compare the temperature dependences of the thermal energy (E_p) and heat capacity (C_p), obtained from MD simulations based on quantum FDR vs classical FDR (CFDR). The difference at low temperatures due to the use of quantum statistics and the agreement beyond the Debye temperature are both expected. The nonzero energy at 0 K for the quantum model comes from the zero-point energy of the phonons, and the corresponding heat capacity in Fig. 1(b) correctly tends to zero at 0 K. Comparison with analytic results obtained from a pure harmonic model in Eq. (23) shows almost perfect agreement at low temperatures. Deviations at high temperatures are due to anharmonic effects in the MD results and are expected. Comparison with simulations using the on-the-fly color-noise quantum bath [12,29] shows excellent agreement and supports the consistency between the two schemes. Good accuracy of the heat capacity over the whole temperature range also implies reliability of the entropy and free energies calculated from this scheme for atomic processes.

B. Energy and specific heat of the spin system from SD simulation

Magnon thermal energy (E_m) and heat capacity (C_m) obtained from spin dynamics simulations are shown as functions of temperature in Figs. 3(a) and 3(b). Results of

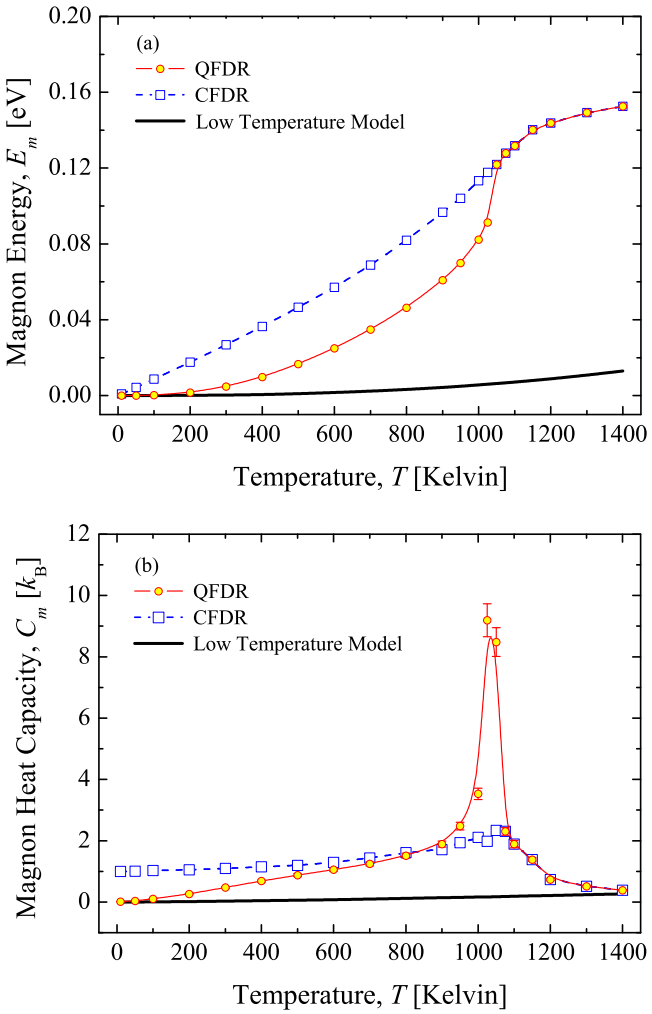

FIG. 3. (Color online) (a) The thermal energy E_m and (b) the specific heat C_m due to spin vibrations computed by SD simulations using quantum (blue open squares, QFDR) and classical (red open circles, CFDR) fluctuation-dissipation relation schemes. Results from the 0-K harmonic model using Eqs. (17) and (30) (black solid line) are also plotted for comparison.

the analytic low-temperature model from Eqs. (18), (27), and (30) with cutoff temperature given by Eq. (26) are also presented for reference. Agreement between low-temperature SD results based on QFDR and the harmonic low-k model is expected. Near T_C, compression of the magnon energy spectrum drastically reduces quantization effects and the difference between classical and quantum results disappears. In this temperature regime, the strong temperature dependence of the magnon thermal energy can be seen from the large difference between the results of the QFDR and the harmonic low-k model (calculated using the 0-K $m-$DOS).

It is clear that CFDR overestimates the thermal energy due to magnon excitation in almost the entire ferromagnetic region [see Fig. 3(a)]. The corresponding heat capacities calculated from the thermal energies are shown in Fig. 3(b). The heat capacity calculated using QFDR can be seen to vanish at 0 K and dramatically increase with temperature over 800 K. The corresponding results based on CFDR remain at 1 k_B at 0 K,

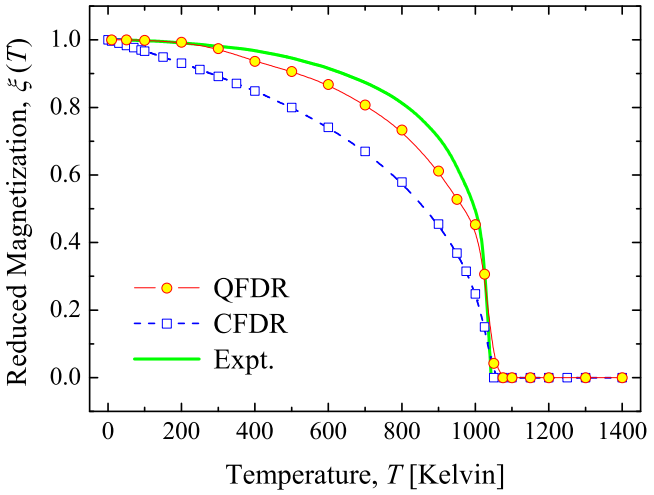

FIG. 4. (Color online) Reduced magnetization $\xi(T) = M(T)/M_0$ using quantum (blue open squares, QFDR) and classical (red open circles, CFDR) fluctuation-dissipation-relation schemes. Plotted for comparison are the experimental data [30] (green solid line).

as required by the classical equipartition theorem. Both the CFDR and QFDR results show similar singular behaviors near the magnetic phase boundary, which is consistent with the characteristics of a second-order phase transition. Yet, the peaking discontinuity is more pronounced with the quantum heat bath, where effects due to the reduction of magnetic order are properly taken care of. Values of $\sim 0.5\,k_B$ in the paramagnetic phase come from the short-range magnetic order. This is consistent with results based on CFDR. Such peaking behavior, however, is completely absent from the harmonic model. We note that the temperature dependence of the DOS has much stronger effects in the spin system than that in lattice system.

The temperature dependences of the reduced magnetization $\xi(T)$, i.e., $\xi(T) \equiv M(T)/M_0$, using quantum and classical temperature controls are compared in Fig. 4, together with experimental data [30]. The difference between the quantum and classical results is clear, as well as the improved agreement between the experimental and calculated reduced magnetization.

It is the use of Bose-Einstein, instead of Boltzmann, distribution in the QFDR in Eq. (19) that is responsible for the better agreement of our results with the experimental data at low temperatures, e.g., $T < 300$ K. On the other hand, the good agreement between the experimental and theoretical Curie temperatures, quantum or classical, comes from the disappearance of quantization effects on the emulating noise when the corresponding magnon energy spectrum is compressed due to magnon softening. At the same time, the faster reduction of the magnetization near T_C is due to the use in Eq. (33) of a temperature-dependent spin stiffness, which follows from the scaling laws of phase transition, in the magnon DOS in the QFDR in Eq. (19). Thus the improved agreement with experiments is traceable to the use of a QFDR based on a temperature-dependent DOS in the Bose-Einstein statistics of temperature-dependent magnons.

This does not contradict the well-known fact that mean-field theory is good enough to describe the temperature dependence of magnetization near the magnetic phase boundary but fails at low temperatures [31].

C. Spin-lattice dynamics simulation

In Figs. 5(a) and 5(b) we compare the temperature dependences of the energies and heat capacities of bcc iron, calculated using SLD simulations based on quantum and classical heat baths, respectively. Experimental data [32] and results from the analytical low-k model are also plotted for comparison. In these calculations, two thermal heat baths, each following a different fluctuation-dissipation ratio, have to be simultaneously applied to the lattice and spin systems.

In Figs. 5(a) and 5(b), excellent agreement among all the quantum results and experimental ones is seen at low temperatures. The nonlinear temperature dependence of the thermal energy and heat capacities that vanish at 0 K are results of quantization via the use of Bose-Einstein statistics in the QFDR, which are absent in the CFDR results. At higher temperatures, reduction of quantization effects produces results that are more consistent with classical statistics. It is worth noting that, compared with heat capacities calculated based on CFDR, those obtained with QFDR have much better agreement with experiments [32]. At low temperatures, they have the correct temperature dependence $\lim_{T\to 0} C_{\rm tot}(T) = 0$, which is in marked contrast to the lack of temperature dependence obtained when CFDR is used.

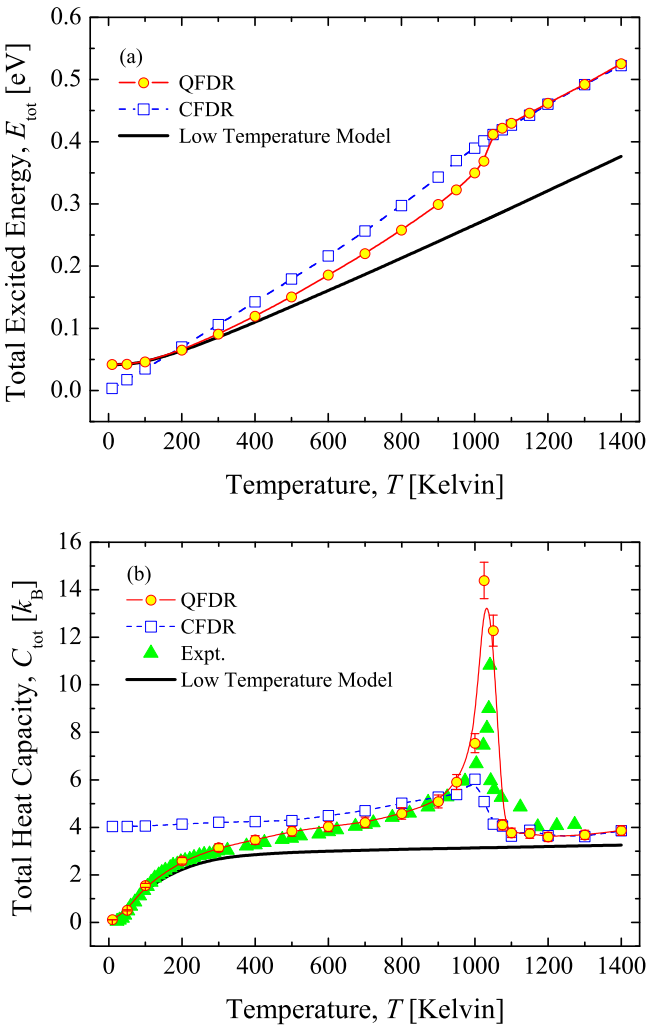

FIG. 5. (Color online) (a) Total lattice and magnetic thermal energies $E_{\rm tot}$ and (b) specific heat $C_{\rm tot}$ computed by SLD simulations using quantum (blue open squares, QFDR) and classical (red open circles, CFDR) fluctuation-dissipation relation schemes. Results from the 0-K harmonic model (black solid line) and experimental data [32] (green triangles) are also plotted for comparison.

At the same time, CFDR and QFDR results in Figs. 5(a) and 5(b) exhibit similar behavior near the Curie temperature. In particular, both show the typical peak in the heat capacities near the second-order magnetic phase transition. Here it should be noted that D_0 and T_C do not even appear anywhere in the CFDR case. On the other hand, in the harmonic models in Figs. 3(b) and 5(b), the Curie point and the singular behavior near it is completely absent even if the QFDR is used. This is a clear indication that the singular behavior near the Curie point in Figs. 3(b) and 5(b) comes directly from the fully anharmonic SD and SLD calculations, and is related intrinsically to the anharmonicity of the Heisenberg Hamiltonian rather than the quasiharmonic treatment in QFDR.

VIII. SUMMARY AND CONCLUSIONS

Quantum effects in the vibrational thermodynamics have to be considered in atomistic simulations of metals in the ferromagnetic phase due to the quantization of spin waves. In this regard, the basis of temperature control in spin and lattice dynamic simulations is reconsidered. Relations between the fluctuation-dissipation ratio and the thermodynamic temperature are reestablished based on the Bose-Einstein statistics within temperature-dependent phonon and magnon pictures. The frequency dependence is absorbed in the corresponding phonon and magnon DOS. In the magnon case, effects on the magnon DOS caused by the Van Hove singularity and magnon softening at the Curie temperature have to be considered in addition. The quantum heat baths are tested in molecular dynamics, spin dynamics, and spin-lattice dynamics simulations. The results are in good agreement with experimental observations and theoretical predictions over a wide temperature range from 0 K to above the Curie temperature of ferro-/paramagnetic transition. Comparison with corresponding simulation results based on classical heat bath confirms that quantum statistics is important in the entire ferromagnetic phase.

ACKNOWLEDGMENTS

This work was supported by Grant No. 11214114 from the Hong Kong Research Grant Commission. Work by S. L. Dudarev and P.-W. Ma has been carried out within the framework of the EUROfusion Consortium and has received funding from the Euratom research and training programme 2014–2018 under Grant agreement No. 633053 and from the RCUK Energy Programme (Grant No. EP/I501045). The views and opinions expressed herein do not necessarily reflect those of the European Commission. This work was also partly

funded by the United Kingdom Engineering and Physical Sciences Research Council via Grant No. EP/G050031.

APPENDIX: THE MEAN ENERGY OF SPIN ENSEMBLE

The average energy $\langle E\rangle$ of the spin system is given by

$$\langle E\rangle = -\frac{1}{2}\sum_{n,m} J_{nm}\,\langle \boldsymbol{S}_n\cdot\boldsymbol{S}_m\rangle = -\frac{1}{2}\sum_{n}\langle \boldsymbol{S}_n\cdot\boldsymbol{H}_n\rangle, \quad \text{(A1)}$$

where the effective field $\boldsymbol{H}_n$ acting on the nth spin is given by $\boldsymbol{H}_n = \sum_{m\neq n} J_{nm}\boldsymbol{S}_m$. Averaging over all atoms, we may define the mean effective field $\boldsymbol{H}$ by

$$\boldsymbol{H} \equiv \langle \boldsymbol{H}_n\rangle = \sum_m J_{nm}\,\langle \boldsymbol{S}_m\rangle = \sum_m J_{nm}\,\langle \boldsymbol{S}\rangle. \quad \text{(A2)}$$

We note that $\boldsymbol{H}$ is strongly temperature dependent via $\langle \boldsymbol{S}\rangle$, which is directly proportional to the crystal magnetization (see Sec. II A). The last equality in Eq. (A2) implies that in equilibrium the average spin vector $\langle \boldsymbol{S}_m\rangle$ is the same for all atoms.

Putting $\boldsymbol{H}_m = \boldsymbol{H} + \delta\boldsymbol{H}_m$, $\boldsymbol{S}_m = \langle \boldsymbol{S}\rangle + \delta\boldsymbol{S}_m$, where $\langle \delta\boldsymbol{S}_m\rangle = 0 = \langle \delta\boldsymbol{H}_m\rangle$, we may write

$$\sum_m J_{nm}\langle \boldsymbol{S}_m\cdot\boldsymbol{H}_m\rangle = \langle \boldsymbol{S}\rangle\cdot\boldsymbol{H}\sum_m J_{nm} + \sum_m J_{nm}\langle \delta\boldsymbol{S}_m\cdot\delta\boldsymbol{H}_m\rangle. \quad \text{(A3)}$$

Within the quasiharmonic approximation, we may neglect the second-order fluctuation terms of Eq. (A3) and write

$$\sum_m J_{nm}\,\langle \boldsymbol{S}_m\cdot\boldsymbol{H}_m\rangle \cong \langle \boldsymbol{S}\rangle\cdot\boldsymbol{H}\sum_m J_{nm} = H^2. \quad \text{(A4)}$$

According to chap. 7 in Ref. [18], neglecting terms second order in fluctuations means that all spins are effectively interacting with the uniform field $\boldsymbol{H}$. Within this approximation, $\boldsymbol{H}_n \cong \boldsymbol{H}$, and

$$\langle \varepsilon_n\rangle = -\langle \boldsymbol{S}_n\cdot\boldsymbol{H}_n\rangle \cong -\frac{\int \boldsymbol{H}\cdot\boldsymbol{S}_n \exp(\beta\boldsymbol{H}\cdot\boldsymbol{S}_n)\,\mathrm{d}^3\boldsymbol{S}}{\int \exp(\beta\boldsymbol{H}\cdot\boldsymbol{S}_n)\,\mathrm{d}^3\boldsymbol{S}}$$

$$= -\frac{\int_{-1}^{1} HS\cos\theta_n \exp(\beta HS\cos\theta_n)\,\mathrm{d}\cos\theta_n}{\int_{-1}^{1}\exp(\beta HS\cos\theta_n)\,\mathrm{d}\cos\theta_n}$$

$$= -\frac{1}{\beta}\frac{\int_{-\beta HS}^{\beta HS} x\exp(x)\,\mathrm{d}x}{\int_{-\beta HS}^{\beta HS}\exp(x)\,\mathrm{d}x} = \frac{1}{\beta}\left[1 - x\coth(x)\right], \quad \text{(A5)}$$

where $x = \beta HS$ and, according to Eq. (13), the spin magnitude S is constant. Thus Eq. (A4) can be written as

$$H^2 = -\frac{H_0}{S}\langle \varepsilon_n\rangle = \frac{H_0}{\beta S}\left[x\coth(x) - 1\right] \Rightarrow H$$

$$= H_0\left(\coth(x) - \frac{1}{x}\right), \quad \text{(A6)}$$

where $H_0 = \sum_m J_{nm}S$ is the amplitude of the effective field of a collinear spin ensemble. We note that spontaneous magnetization requires H to have a nonzero solution, which in turn requires a minimum value for H_0.

The average energy in Eq. (A1) can be evaluated using Eq. (A5). Thus

$$\langle E\rangle = \frac{N\langle \varepsilon_n\rangle}{2} = -\frac{NHS}{2}\left[\coth(x) - \frac{1}{x}\right]$$

$$= -\frac{NH_0S}{2}\left[\coth(x) - \frac{1}{x}\right]^2. \quad \text{(A7)}$$

When $x \gg 1$, $[\coth(x) - \frac{1}{x}]^2 \to 1 - \frac{2}{x}$ and we may, within the quasiharmonic approximation, write

$$\langle E\rangle = \frac{N}{\beta} - \frac{1}{2}NH_0S. \quad \text{(A8)}$$

[1] H. C. Herper, E. Hoffmann, and P. Entel, Phys. Rev. B **60**, 3839 (1999).
[2] N. Ridley and H. Stuart, J. Phys. D: Appl. Phys. **1**, 1291 (1968).
[3] D. J. Dever, J. Appl. Phys. **43**, 3293 (1972).
[4] H. Wen and C. H. Woo, J. Nucl. Mater. **455**, 31 (2014).
[5] P.-W. Ma, C. H. Woo, and S. L. Dudarev, AIP Conf. Proc. **999**, 134 (2008).
[6] P.-W. Ma, C. H. Woo, and S. L. Dudarev, Phys. Rev. B **78**, 024434 (2008).
[7] P.-W. Ma, S. L. Dudarev, A. A. Semenov, and C. H. Woo, Phys. Rev. E **82**, 031111 (2010).
[8] R. Donald, *Einstein's Other Theory: The Planck-Bose-Einstein Theory of Heat Capacity* (Princeton University Press, Princeton, NJ, 2005), p. 73.
[9] M. F. Collins, V. J. Minkiewicz, R. Nathans, L. Passell, and G. Shirane, Phys. Rev. **179**, 417 (1969).
[10] H. A. Mook and R. M. Nicklow, Phys. Rev. B **7**, 336 (1973).
[11] M. Ceriotti, G. Bussi, and M. Parrinello, Phys. Rev. Lett. **102**, 020601 (2009).
[12] H. Dammak, Y. Chalopin, M. Laroche, M. Hayoun, and J.-J. Greffet, Phys. Rev. Lett. **103**, 190601 (2009).
[13] R. Kubo, Rep. Prog. Phys. **29**, 255 (1966).
[14] B. Fultz, Prog. Mater. Sci. **55**, 247 (2010).
[15] C. Kittel, *Introduction to Solid State Physics*, 8th ed. (John Wiley & Sons,Inc., New York, 2005), Chap. 5, pp. 105–130.
[16] V. Fock, Zeitschrift für Physik A **63**, 855 (1930).
[17] C. Kittel, *Introduction to Solid State Physics*, 8th ed. (John Wiley & Sons, Inc., New York, 2005), Chap. 12, pp. 323–360.
[18] P. Mohn, *Magnetism in the Solid State: An Introduction*, Corrected 2nd Printing (Springer, New York, 2006), Chap. 7, pp. 62–74.
[19] J. Van Kranendonk and J. H. Van Vleck, Rev. Mod. Phys. **30**, 1 (1958).
[20] F. Reif, *Fundamentals of Statistical and Thermal Physics* (McGraw-Hill Book Company, New York, 1965), Chap. 10, pp. 404–437.

[21] S. V. Halilov, A. Y. Perlov, P. M. Oppeneer, and H. Eschrig, Europhys. Lett. **39**, 91 (1997).
[22] L. D. Landau and E. M. Lifshitz, Phys. Z. Sowjetunion **8**, 153 (1935).
[23] L. P. Kadanoff, W. Gotze, D. Hamblen, R. Hecht, E. A. S. Lewis, V. V. Palciauskas, M. Rayl, J. Swift, D. Aspnes, and J. Kane, Rev. Mod. Phys. **39**, 395 (1967), (Table VII).
[24] S. L. Dudarev and P. M. Derlet, J. Phys.: Condens. Mat. **17**, 7097 (2005).
[25] B. I. Halperin and P. C. Hohenberg, Phys. Rev. **177**, 952 (1969).
[26] N. Hatano and M. Suzuki, Lect. Notes Phys. **679**, 37 (2005). P.-W. Ma and C. H. Woo, Phys. Rev. E **79**, 046703 (2009).
[27] H. J. C. Berendsen, J. P. M. Postma, W. F. Van Gunsteren, A. Di Nola, and J. R. Haak, J. Chem. Phys. **81**, 3684 (1984).
[28] *American Institute of Physics Handbook*, 3rd ed. edited by D. E. Gray (McGraw-Hill, New York, 1972), pp. 4–115.
[29] J.-L. Barrat and D. Rodney, J. Stat. Phys. **144**, 679 (2011).
[30] J. Crangle and G. M. Goodman, Proc. R. Soc. London, Ser. A **321**, 477 (1971).
[31] P. Mohn, *Magnetism in the Solid State: An Introduction*, Corrected 2nd Printing (Springer, New York, 2006), Chap. 6, pp. 53–61.
[32] D. C. Wallace, P. H. Sidles, and G. C. Danielson, J. Appl. Phys. **31**, 168 (1960).